Microscopic characterization of structural relaxation and cryogenic rejuvenation in metallic

glasses

T.J. Lei¹, L. Rangel DaCosta¹, M. Liu², W. H. Wang², Y. H. Sun², A. L. Greer³, and M. Atzmon^{1,4,*}

¹Department of Materials Science and Engineering, University of Michigan, Ann Arbor, Michigan

48109, USA.

² Institute of Physics, Chinese Academy of Sciences, Beijing, 100080, China.

³ Department of Materials Science & Metallurgy, University of Cambridge, Cambridge, UK.

⁴ Department of Nuclear Engineering and Radiological Sciences, University of Michigan, Ann

Arbor, Michigan 48109, USA.

* Corresponding author: atzmon@umich.edu

Abstract

Plasticity improvement in metallic glasses resulting from cycling treatment between room and

liquid nitrogen temperature has been reported and attributed to rejuvenation due to non-uniform

thermal expansion coefficient. However, the detailed microscopic effect is still unclear. The

present study focuses on the microscopic effect of room-temperature ageing and cryogenic cycling.

La₇₀Cu₁₅Al₁₅ and La₇₀Ni₁₅Al₁₅ metallic glasses were subjected to varying ageing times, after which

some were also cryogenically cycled. Quasi-static anelastic relaxation measurements were then

employed to characterize the time-constant spectra over seven orders of magnitude. The overall

anelastic strain decreases with increasing ageing time, but is not noticeably affected by cryogenic

cycling. On the other hand, while ageing also causes an increase in characteristic time constants,

1

Acta mater., in press

10.1016/j.actamat.2018.10.036

cycling reverses this effect. The new details shed light on the effect of structural relaxation and

rejuvenation on the properties of shear transformation zones.

Keywords

Metallic glasses; Anelastic relaxation spectra; Rejuvenation; Structural relaxation

1. Introduction

Metallic glasses (MGs) have been considered as potential structural materials owing to their high

strength and elastic limit [1]. However, they exhibit little macroscopic plasticity due to shear band

formation, which limits their practical applications [2]. Rejuvenation is one approach to enhancing

the plasticity of MGs, which involves structural excitation and an increase in stored energy [3].

Different methods are used for rejuvenation, such as cyclic elastic loading [4], constrained loading

[5], and irradiation [6,7]. The recent discovery of improved mechanical properties of MGs

resulting from cryogenic cycling between room temperature (RT) and liquid nitrogen temperature

has attracted much attention, since this method is non-destructive, isotropic and controllable

[8,9,10,11]. The authors attributed the effect to a non-uniform structure and associated thermal

expansion coefficient. However, microscopic details are still missing.

Due to their disordered atomic structure, it is challenging to define flow defects in MGs [12,13].

Based on observation of two-dimensional bubble rafts, Argon [14] proposed that atomic clusters,

termed shear transformation zones (STZs) [15], accommodate inelastic deformation of MGs. At

2

small strain, STZs are isolated and can be reversed upon removal of the stress due to the back stress in the elastic matrix, which results in anelasticity. With increasing strain, STZs begin to interact with each other, back stress in the elastic matrix is lost, and the strain is permanent. Numerous experiments and simulations [16,17,18] have been conducted to characterize STZs, with some ambiguous results.

Recently, Ju *et al.* [19] analyzed relaxation-time spectra, $f(\tau)$, obtained from quasi-static anelastic relaxation measurements for an Al-based MG at RT. Since the strain was small, within the nominally elastic regime, STZs were in the dilute limit and did not interact with each other. Two techniques, nanoindenter cantilever bending for short-time measurements and bend relaxation for longer time, were employed to observe the anelastic strain evolution. For the latter, samples were constrained around a mandrel for $2 \cdot 10^6$ s, then relaxed stress-free. The evolution in radius of curvature was then monitored from $\sim 10^3$ s to $3.1 \cdot 10^7$ s. Nonlinear least-squares fits were employed to obtain relaxation-time spectra, which exhibited distinct peaks corresponding to different STZ types. The time constant of each type is an increasing function of its volume. Surprisingly, an atomically quantized hierarchy of STZs was observed: the STZ volume values computed for the peaks were spaced by the atomic volume of Al, the majority element.

In this paper, we use a similar approach to study the effect of RT ageing and cryogenic cycling on two La-based MGs by characterizing their anelastic time-constant spectra at RT. The magnitude of the anelastic strain induced after ageing decreases with increasing ageing time, at a relative rate that varies with the corresponding time constant. Cryogenic cycling, after ageing and prior to

anelastic deformation, does *not* change the magnitude of the strain. Ageing also increases the relaxation time constants and results in more-distinct spectrum peaks – trends that *are* reversed by cycling. These observations are discussed in terms of STZ properties.

2. Experiment and analysis procedure

Two alloy compositions, La₇₀Cu₁₅Al₁₅ and La₇₀Ni₁₅Al₁₅ (at. %), have been investigated. Their glass transition temperatures are 391 K and 431 K, respectively [20]. Ribbons \sim 40 μ m thick and 1 mm wide, were obtained by single-wheel melt-spinning, using a Cr-coated Cu wheel, at a tangential velocity of \sim 3 m/s in an argon atmosphere with a pressure of 20 kPa. X-ray diffraction was employed to confirm the amorphous structure. Since these alloys undergo structural relaxation at RT, samples with RT (293 \pm 1 K) ageing time ranging from 1.9·10⁶ s to 2.9·10⁷ s were used, 3-8 samples for each condition. Samples aged for 1.0·10⁷ s were also subsequently cycled between RT and liquid nitrogen temperature ten times, with 3 minutes and 1-minute holding time, respectively.

The following thermomechanical treatment and measurement sequence was applied to 1 cm long ribbon segments, as also illustrated in Fig. 1: After ageing with or without subsequent cryogenic cycling, bend-relaxation measurements were performed at RT. Samples were constrained around mandrels of radii R ranging from 0.348 cm to 0.802 cm for a standard time of $2.0 \cdot 10^6$ s. Subsequently, the stress-free evolution of radius of curvature, r(t), was monitored for up to $2.6 \cdot 10^7$ s using a digital camera, taking care to align its optical axis perpendicular to the sample plane. An automated image analysis method was developed for curvature determination, significantly

reducing the error bars in the strain vs. time curves. The maximum equilibrium elastic strain at the end of the constraining period, and the anelastic strain at time t after constraint removal, both attained at the surface, are $\varepsilon_{el}^0 = d/2 \cdot [1/R - 1/r(0)]$ and $\varepsilon_{an}(t) = d/2 \cdot [1/r(t) - 1/r_0]$, respectively, where d is the sample thickness and r_0 is the radius of curvature before constraint [19].

In order to estimate the effect of cryogenic treatment on elastic properties, Young's modulus was measured. RT tensile tests were performed at a strain rate of 10⁻³ s⁻¹, using a TA Instruments RSA III Dynamic Mechanical Analyzer. Pairs of neighboring ribbon segments with identical ageing time were used. One segment of each pair was also subjected to 10 cryogenic cycles after ageing. Uncertainty in sample dimensions was thus essentially canceled out in the relative difference in modulus. Four sample pairs were used for each alloy type and ageing time.

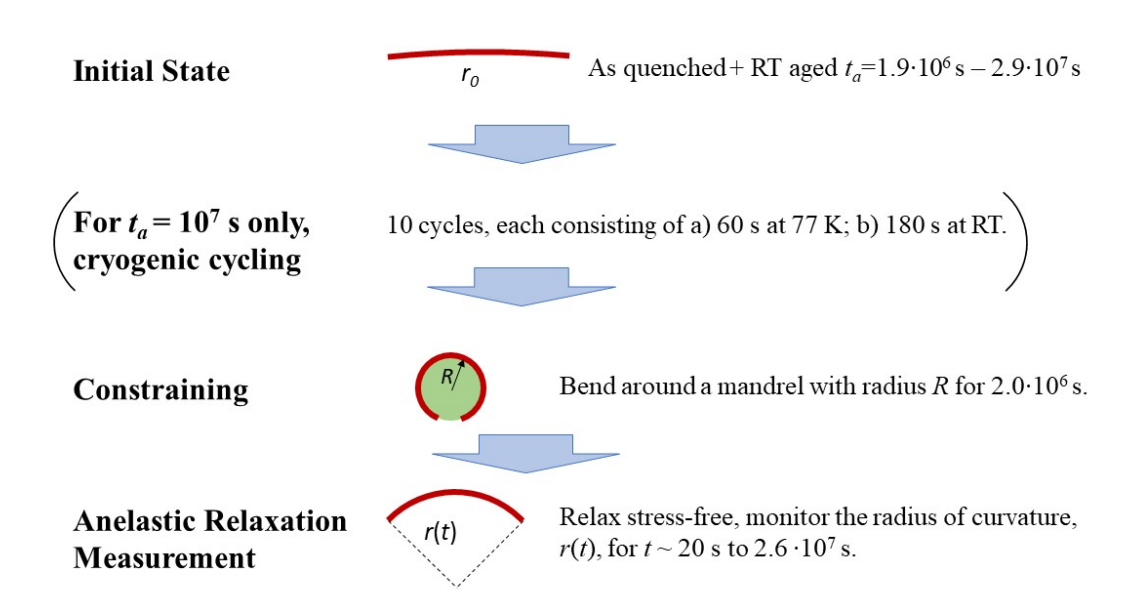


Figure 1. Schematic illustration of the thermomechanical treatment and measurement sequence.

To obtain relaxation-time spectra $f(\tau)$, CONTIN, a portable package for inverse problems, was employed to yield stable and consistent fitting of $\varepsilon_{an}(t)/\varepsilon_{el}^0$ [21,22]: based on a linear solid model [19], $\varepsilon_{an}(t)/\varepsilon_{el}^0 = c_{\infty} + \sum_{i=1}^{N} \varepsilon_i \exp(-t/\tau_i)$, where c_{∞} and ε_i are fitting parameters. The relaxation-time values, τ_i , $i=1, \ldots, N=50$, less than the number of data points, are logarithmically spaced. The continuous spectra were approximated as:

$$f(\tau_i) = \varepsilon_i / \Delta \ln \tau, \tag{1}$$

where $\Delta \ln \tau = \ln[\tau_{max}/\tau_{min}]/(N-1)$ with $\tau_{min} = 10$ s and $\tau_{max} = 5.2 \cdot 10^7$ s. The additive term, c_{∞} , was included in the fits to account for processes with time constants longer than τ_{max} . A regularization term was used in the optimization procedure [21,22], which eliminates sharp, unphysical, variations in the spectrum due to numerical artifacts. For consistency, similar regularization parameters were used for all samples. Within a range of regularization parameter values, the spectrum does not change significantly. Ref. [19] contains further details on fitting and consistency checks.

The normalization of $f(\tau)$ in Eq. (1) was chosen for convenient analysis on a logarithmic scale [19,23] since the time constants spanned several orders of magnitude. $\varepsilon_{an}(t=0)/\varepsilon_{el}^0 = \int_0^\infty f(\tau) d\ln \tau$. $\int_{\tau_1}^{\tau_2} f(\tau) d\ln \tau$ is equal to the normalized anelastic strain with time constants in the range (τ_1, τ_2) . According to Ref. [19], this latter integral is also equal to the volume fraction occupied by *potential* STZs with time constants in the corresponding range. *Potential* STZs are clusters of atoms capable of undergoing a shear transformation. Finally, peak properties were determined from an average over all samples for a given history. The error bars are the standard deviations of the mean.

3. Results and discussion

Figure 2 shows representative normalized anelastic strain relaxation data, $\varepsilon_{an}(t)/\varepsilon_{el}^0$, for La₇₀Cu₁₅Al₁₅ and La₇₀Ni₁₅Al₁₅ ribbons, aged for different lengths of time, with and without cryogenic cycling treatment prior to bending. One observes a remarkable decrease of $\varepsilon_{an}(t=0)/\varepsilon_{el}^0$ with structural relaxation: The "youngest" sample, aged $1.9 \cdot 10^6$ s, exhibits the largest value of $\varepsilon_{an}(0)/\varepsilon_{el}^0$, 1.24 and 0.67 for La₇₀Cu₁₅Al₁₅ and La₇₀Ni₁₅Al₁₅, respectively, as compared with 0.35 and 0.20 for ageing time of $2.9 \cdot 10^7$ s. This observation implies that structural relaxation leads to a significant decrease of the volume fraction occupied by *potential* STZs. It is noteworthy that the initial anelastic strain of the "youngest" La₇₀Cu₁₅Al₁₅ sample is greater than the elastic strain, ε_{el}^0 . Cryogenic cycling does not affect $\varepsilon_{an}(0)/\varepsilon_{el}^0$, as discussed further below.

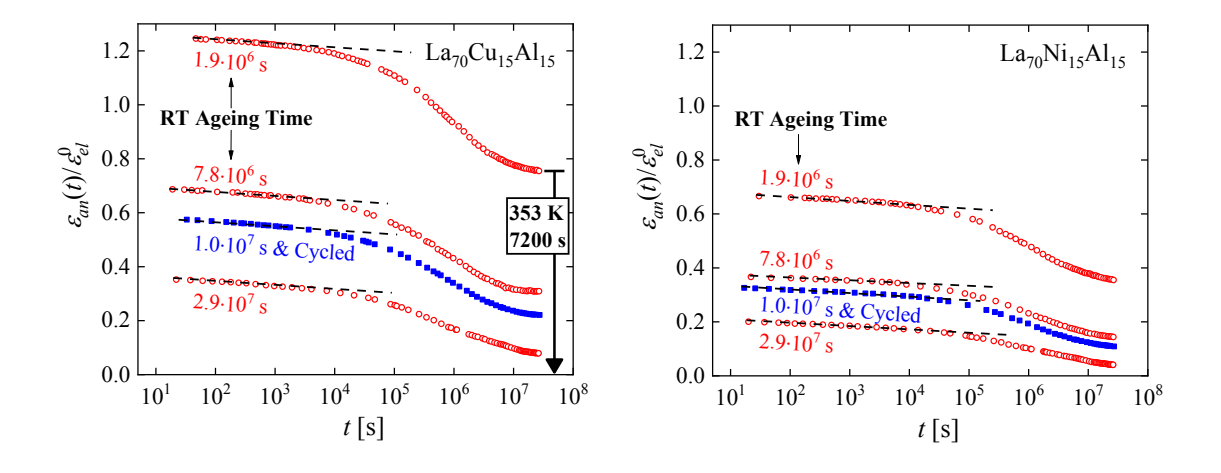


Figure 2. Normalized anelastic strain of La₇₀Cu₁₅Al₁₅ and La₇₀Ni₁₅Al₁₅ as a function of time for different ageing times prior to bending, as indicated. Open circles and filled squares correspond, respectively, to measurements without and with cryogenic cycling after ageing, prior to bending. Curves are not shifted. The dashed lines are all drawn with the same slope. Note that the entire strain is anelastic, as verified by annealing at temperature above RT (bold arrow).

The following discussion addresses the details of the effect of ageing on potential STZs, as resolved by their size/time constant. At short measurement time, up to $\sim 10^4$ s, the absolute strain relaxation rate is the same for varying prior thermal history, as indicated by the dashed lines, all drawn with the same slope. However, the strain evolution at longer time depends on the prior ageing time, as "younger" samples have higher strain that decreases faster. Comparing the two alloys at the same ageing time, the overall strain magnitude of La₇₀Cu₁₅Al₁₅ is higher than that of La₇₀Ni₁₅Al₁₅. However, the slope at short measurement time is very similar for both alloys, as indicated by the dashed lines. This indicates that the difference in strain between the two alloys is mainly due to STZs with large time constants. The large amount of strain at the end of the measurement time could be either permanent or anelastic with time constants greater than those measured. However, annealing for 7200 s at 353 K restored the radius of curvature to its initial value, r_0 (See Fig. 2), proving that the entire strain measured is anelastic. These observations are a manifestation of the fact that anelastic processes with large time constants can be induced during a much shorter time. In summary, we observe a significant effect of alloy composition and structural relaxation on the anelastic strain magnitude, and on its evolution rate for $t \ge 10^4$ s.

The effect of cryogenic cycling on anelastic relaxation is not obvious in Fig. 2. Ideally, one would compare samples aged for the same duration with and without subsequent cryogenic cycling treatment. We have observed the same value, within error, of $\varepsilon_{an}(t=0)/\varepsilon_{el}^0$ for samples aged $6.2 \cdot 10^7$ s with and without cryogenic cycling. Among samples for which we have full $\varepsilon_{an}(t)$ data, the ageing time of samples with cryogenic cycling is $1.0 \cdot 10^7$ s, and the closest ageing time of samples without cycling is $7.8 \cdot 10^6$ s. The trends with ageing time will allow us to further examine the effect of cycling. In Ref. [8], the compressive plastic strain of MGs increases significantly by

successive cryogenic cycles. This effect is strongest for partially relaxed samples, and insignificant for fully relaxed samples. In contrast, in the present study, in which all samples are partially relaxed, cycling does not cause any noticeable deviation from the trend in anelastic strain magnitude with ageing. Further details are now examined by computing the spectra corresponding to Fig. 2.

Figure 3 shows the relaxation-time spectra computed from Fig. 2, shifted vertically for clarity. Two representative spectra are shown for each temperature history, demonstrating reproducibility. All spectra exhibit distinct peaks, which we associate with distinct STZ types, numbered $m=1, 2, \ldots, 6$ (see below), based on shape similarity between spectra. It should be noted that 3 out of 8 samples with cryogenic cycling show subtle shoulders at large time constants for each alloy. Because of uncertainty in the spectra, we do not consider these shoulders significant.

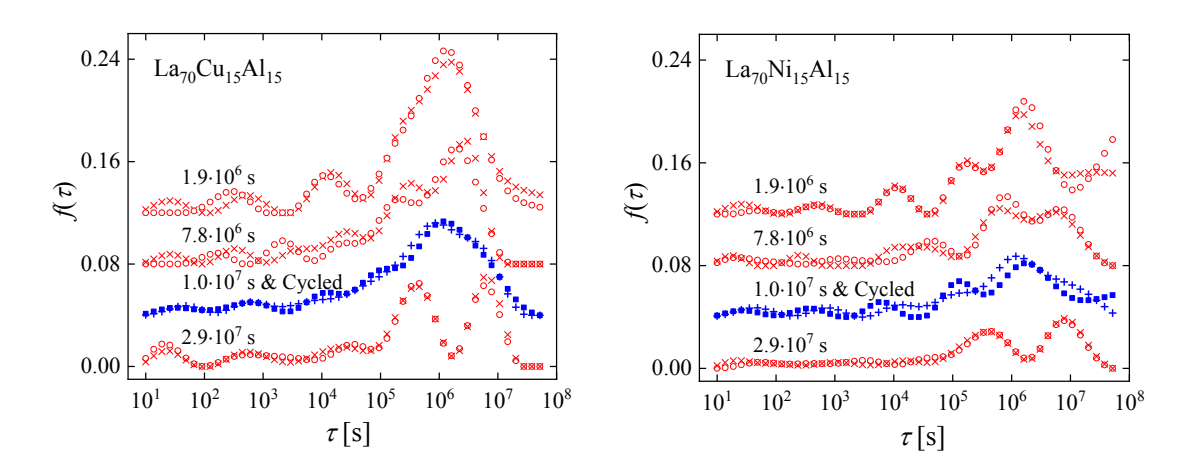


Figure 3. Relaxation-time spectra for La₇₀Cu₁₅Al₁₅ and La₇₀Ni₁₅Al₁₅ with different ageing times, as indicated. For each condition, representative data for two independent samples are shown. Open circles and crosses, vs. filled squares and pluses, correspond to samples without, vs. with, cryogenic cycling, respectively. The curves are shifted vertically for clarity.

With increasing ageing time, for samples without cryogenic cycling, the peak positions shift to longer time, while their intensities decrease. The last two peaks also become more distinct. The spectra for samples aged $1.0 \cdot 10^7$ s and cryogenically cycled resemble those for the "youngest" samples (aged $1.9 \cdot 10^6$ s) in peak position and shape: cycling has reversed the ageing-induced increase in time constants, and for La₇₀Cu₁₅Al₁₅, it also re-blurred the peaks. It should be noted that this is not an artifact of data quality or spectrum computation: samples with cryogenic cycling yield fits of equal quality, and similar regularization parameters are used for all samples.

In agreement with the strain curves, the peak intensities for large time constants for La₇₀Cu₁₅Al₁₅ in Fig. 3 are in general higher than for La₇₀Ni₁₅Al₁₅. As an aside, this is the reason that the high frequency beta relaxation in the loss modulus appears more pronounced in La₇₀Ni₁₅Al₁₅ than in La₇₀Cu₁₅Al₁₅ [24], since it is common to normalize loss modulus data by the peak height of the slower alpha relaxation. The spectra in Fig. 3 correspond to the slow alpha relaxation, whereas the faster beta relaxation has τ values generally below those in Fig. 3. Spectra corresponding to such τ values have been obtained from nanoindenter cantilever measurements, and will be presented elsewhere [25].

As in Ref. [19], we interpret the spectrum peaks as representing an atomically quantized hierarchy of STZs, and expect further peaks above 10^8 s, if measured. Ju *et al.* [19] showed that the area of peak m, $c_m = \int_m f(\tau) d \ln \tau$, is equal to the volume fraction occupied by *potential m*-type STZs. As seen in Figs. 2 & 3, the main contributions to the anelastic strain are due to the high end of the spectrum, above $\sim 10^4$ s, plus the yet slower STZs represented by the constant term, $c_\infty (= \sum_{m>6} c_m)$,

used in the spectrum fit for $\varepsilon_{an}(t)/\varepsilon_{el}^0$. The latter STZs would only be visibly reversed over times longer than the measurement time used, or at elevated temperature (see above).

In order to further examine the effect of ageing and cryogenic cycling, the following are shown in Fig. 4 as a function of RT ageing time: a) the volume fraction occupied by *potential* STZs of all types, m, given by $c_{total} = \varepsilon_{an}(t=0)/\varepsilon_{el}^0$, which is equal to c_{∞} plus the integrated area of the entire spectrum [19]; b) the volume fraction occupied by *potential* m=5 & m=6 STZs, $c_{5,6}$, equal to the integrated area of the corresponding peaks; c) the volume fraction, c_{∞} , occupied by *potential* STZs with $\tau > \tau_{max}$. Note that $c_{total} > 1$ for La₇₀Cu₁₅Al₁₅ (Fig. 2) is physically meaningful, as discussed in Ref. [19], since the definition of c is based on multiple counting of volume elements contained in more than one *potential* STZ. The error bars in Fig. 4 are small, indicating reproducibility. All curves decrease with increasing ageing time, but c_{∞} , the contribution due to time constants larger than those included in the spectrum, clearly decreases at a higher absolute or relative rate than $c_{5,6}$ does. Samples with cryogenic cycling fit well the trend of each curve, indicating that cryogenic cycling prior to bending has not noticeably affected the volume fraction occupied by *potential* STZs of any type/size. Also, as mentioned above, for samples aged $6.2 \cdot 10^7$ s, cryogenic cycling does not affect $c_{total} = \varepsilon_{an}(t=0)/\varepsilon_{al}^0$.

It is likely that each c_m evolves with ageing time, t_a , as $c_{m,\infty}^0 + g_m(t_a)$, where $c_{m,\infty}^0$ is the limiting value for the glass at internal equilibrium, and $g_m(t_a)$ is a function that decays to zero at long time. The small number of data points in Fig. 4 is insufficient for determining detailed ageing kinetics

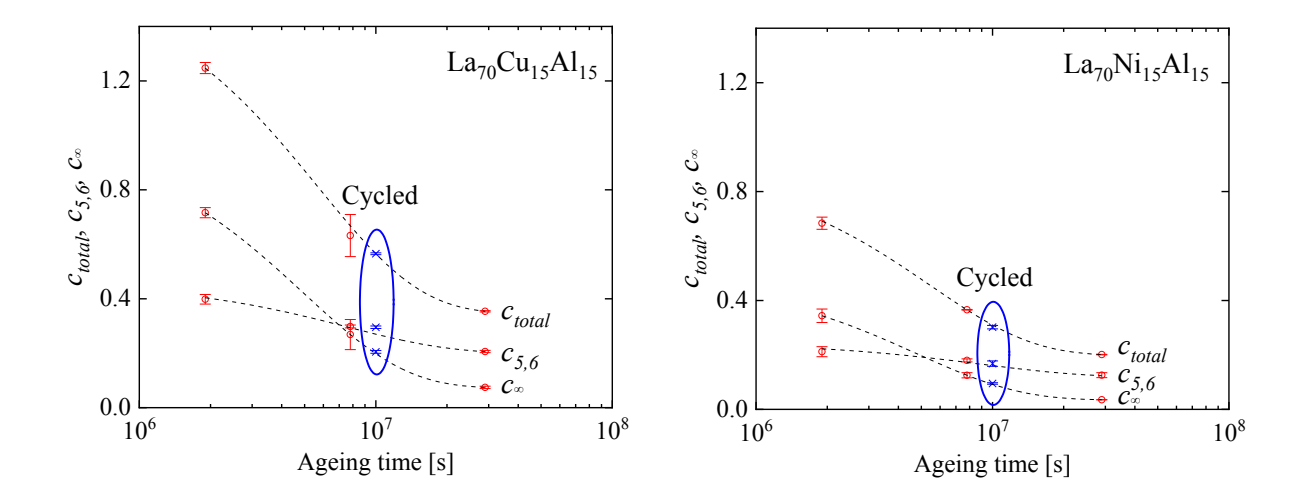


Figure 4. c_{∞} , = the additive term in the spectrum fit, $c_{5,6}$ = the integrated area of the last two peaks, and c_{total} = the integrated area of the entire spectrum plus c_{∞} vs. aging time for La₇₀Cu₁₅Al₁₅ and La₇₀Ni₁₅Al₁₅ MGs. Lines are a guide to the eye.

for each STZ type or range of τ . However, it is clear that $g_m(t_a)$ consists of contributions with time constants much longer than the corresponding τ_m . For example, c_∞ , the sum of the contributions with time constants $\tau > \tau_{max}$ decreases dramatically during ageing times shorter than 10^7 s. In other words, one cannot directly associate the time constant for a particular anelastic process with its time constant for ageing. We note that while $c_\infty = (\sum_{m>6} c_m) > (c_5 + c_6)$ for short ageing times, the reverse is true for long ageing times, and it appears that $\sum_{m>6} c_{m,\infty}^0 \ll (c_{5,\infty}^0 + c_{6,\infty}^0)$.

The analysis we present above assumes implicitly that all anelastic processes reach mechanical equilibrium during the constraining period. Since the constraining time is shorter than the largest time constants that affect measured evolution, it is important to consider the effect of deviations from mechanical equilibrium at the end of the constraining time on c values. We first note that the

deviation should be smaller than expected from the time constants: Ju *et. al.* [19] calculated the correction to c_8 for the linear solid model used, but later measurements [26] showed that this correction was a large overestimate. (This suggests that the behavior under constraint cannot be perfectly described by the linear solid model.) For RT ageing times less than $2.9 \cdot 10^7$ s, the time constants are smaller than the constraining time, so equilibration can be assumed. For both alloy compositions with RT ageing time $2.9 \cdot 10^7$ s, one expects m=6 STZs to not equilibrate with the elastic strain within the constraining time $t_c \ll \tau_6$. As a result, the data corresponding to that ageing condition are underestimated in Fig. 4. However, the underestimation is insignificant, as we conclude from the cryogenically cycled sample: c values (c_{total} , $c_{5,6}$, and c_{∞}) corresponding to samples with cryogenic cycling still follow the trend of the samples without cryogenic cycling even though their time constants decreased by cryogenic cycling. Based on this discussion, we can also safely assume that for τ_l with $i \le 5$, their shift does not affect the measured c_l .

Figure 5 shows the evolution with ageing of the time constants, τ_m , obtained as the median of each spectrum peak m. As mentioned above, m values were assigned based on the similar shape of spectra corresponding to different ageing times. The time constants increase with increasing ageing time for samples without cycling. The effect of cryogenic cycling is indicated with arrows, except when m assignment is too uncertain for small m for La₇₀Cu₁₅Al₁₅. A clear trend of decreasing time constants with cryogenic cycling is seen, reversing the prior ageing effect, as also seen in the qualitative features of the spectra.

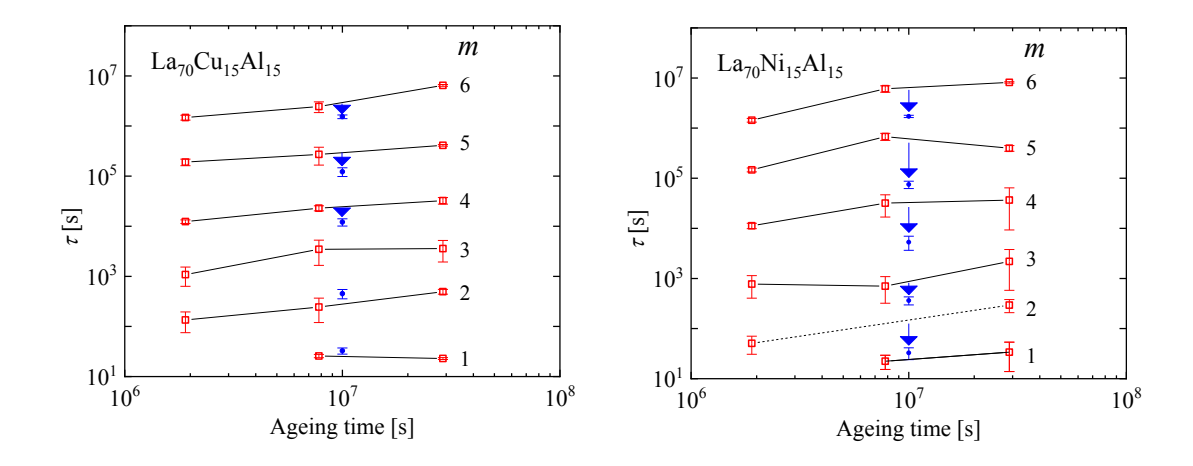


Figure 5. The evolution of time constants of different STZ types, *m*, with ageing time for La₇₀Cu₁₅Al₁₅ and La₇₀Ni₁₅Al₁₅ MGs. Arrows indicate the effect of cryogenic cycling.

Ref. [26] reports that for an Al-based MG, annealing at 383 K for 3600 s prior to anelastic relaxation measurement only decreased c_m , but left the peak position unchanged. It followed that structural relaxation only decreased the number of *potential* STZs, without changing their properties. In the present study, too, we observe a decrease in number of *potential* STZs with ageing. This trend is *not* reversed by cryogenic cycling. Unlike in Ref. [26], the time constants increase with increasing ageing time for the present La-based MGs. This increase is completely reversed after cryogenic cycling, pointing to a rejuvenation effect.

The cause of the observed changes in time constant are discussed next. The time constant for an elastic relaxation due to STZs of volume Ω_m is given by [19] as:

$$\tau_{m} = \frac{3\eta'_{m}}{E'_{m}} = \frac{1}{\mu\Omega_{m}} \cdot \frac{3kT}{2(1+\nu)\gamma_{0}^{c}v_{G}\gamma_{0}^{T}} \cdot \exp\left(\mu\Omega_{m} \cdot \left\{\frac{\gamma_{0}^{T}}{kT} \cdot \left[\left(\frac{(7-5\nu)}{30(1-\nu)} + \frac{2(1+\nu)}{9(1-\nu)}\bar{\beta}^{2}\right)\gamma_{0}^{T} + \frac{1}{2} \cdot \frac{\overline{\sigma_{STZ}}}{\mu}\right]\right\}\right), \tag{2}$$

where η'_m is the effective shear viscosity, E'_m is the effective Young's modulus. $\gamma_0^c = [2(4-5v)/15(1-v)]\gamma_0^T$ is the transformation shear strain of a constrained STZ with $\gamma_0^T = 0.2$ being the unconstrained transformation shear strain. v_G is the attempt frequency, k is the Boltzmann's constant and T is the temperature. v is Poisson's ratio, $\bar{\beta}^2$ is the dilatancy factor, $\bar{\sigma}_{STZ}$ is the shear resistance of the STZ and μ is the shear modulus. Since structural relaxation involves insignificant volume changes, the most likely cause of a shift in time constants is a change in the shear modulus. Based on Eq. (2), the present results are consistent with an increase of ~5% in shear modulus [25,27].

In order to confirm the role of the shear modulus, Young's modulus was measured. In essentially identical samples, it was lower by 3-7% for samples subjected to cryogenic cycling. No clear trend in this change with composition was observed. Since relative changes in Young's modulus and shear modulus upon structural relaxation have been shown to be very similar [28], this result supports an interpretation that the changes in time constants are due to changes in the shear modulus. In light of the report by Ketov *et al.* [8] that cryogenic cycling of La₅₅Ni₂₀Al₂₅ MG did *not* change its Young's modulus, further support is given by our observation [25] that cycling led to slight broadening, but no shift, in spectrum peaks for the same alloy. This points to a significant dependence of the behavior on composition.

While a quantitative evaluation of peak widths is not possible for the present data, we observe for La₇₀Cu₁₅Al₁₅ evolution toward more-distinct peaks with ageing, which is reversed by cycling. This trend could be influenced by differential changes in position, height and shape of each peak. The

latter would point to structural homogenization due to ageing, and the reverse upon cryogenic cycling.

Atzmon and Ju [26] modeled the details of the spectrum of time constants and its change with structural relaxation on the basis of a single parameter – the free volume. The present complex observations are a strong reminder that structural relaxation and rejuvenation cannot be described with a single parameter [29]. We finally note that for a given shear modulus, the present data also yield an STZ volume value for each spectrum peak, as in Ref. [19]. When cantilever measurements of smaller time constants are included, two regimes of volume increment are observed in the STZ hierarchy, which is important for understanding the beta relaxation. This aspect of the study will be published elsewhere [25].

It would be highly desirable to model the observed behavior with atomistic simulations. Since STZs are thermally activated, the time scale accessible by conventional molecular dynamics is far too short for this purpose. Recent work [18,30] has demonstrated progress in atomistic simulations of glass behavior on longer time scale, and the authors hope it would lead to future simulations of the phenomena they report.

4. Conclusions

An unprecedented, detailed, description of the effects of structural relaxation, and rejuvenation by cryogenic cycling, has been obtained. Some of the effects of RT ageing are reversed by cycling,

but others are not. RT ageing increases the time constants for anelastic relaxation significantly. It also de-blurs the spectrum features for La₇₀Cu₁₅Al₁₅ for long time constants, 10^5 to $>10^7$ s at room temperature. Both effects are reversed by cryogenic cycling, thus exhibiting a rejuvenation effect. The observed changes in time constants are likely due to changes in the shear modulus. Ageing also significantly reduces the volume fraction occupied by *potential* STZs, especially of those with time constants greater than the measurement duration of $2.6 \cdot 10^7$ s. This loss is not recovered by cryogenic cycling. These detailed results are expected to provide important insights into the effects of both ageing and cryogenic cycling on the ductility of metallic glasses.

Acknowledgements

The authors thank Prof. Eran Bouchbinder for useful discussions. This work was funded by the U.S. National Science Foundation (NSF), Grants Nos. DMR-1307884 and DMR-1708043.

References

[1] T. C. Hufnagel, C. A. Schuh, M. L. Falk, Deformation of metallic glasses: Recent developments in theory, simulations, and experiments, Acta Mater. 109 (2016) 375-393.

[2] C. C. Hays, C. P. Kim, W. L. Johnson, Microstructure controlled shear band pattern formation and enhanced plasticity of bulk metallic glasses containing in situ formed ductile phase dendrite dispersions, Phys. Rev. Lett. 84 (2000) 2901.

[3] P. M. Derlet, R. Maaβ, Thermal processing and enthalpy storage of a binary amorphous solid: A molecular dynamics study, J. Mater. Res. 32 (2017) 2668-2679.

- [4] D. V Louzguine-Luzgin, V. Y. Zadorozhnyy, S. V Ketov, Z. Wang, A. A. Tsarkov, A. L. Greer, On room-temperature quasi-elastic mechanical behaviour of bulk metallic glasses, Acta Mater. 129 (2017) 343-351.
- [5] J. Pan, Y. X. Wang, Q. Guo, D. Zhang, A. L. Greer, Y. Li, Extreme rejuvenation and softening in a bulk metallic glass, Nat Commun. 9 (2018) 560.
- [6] D. J. Magagnosc, G. Kumar, J. Schroers, P. Felfer, J. M. Cairney, D. S. Gianola, Effect of ion irradiation on tensile ductility, strength and fictive temperature in metallic glass nanowires, Acta Mater. 74 (2014) 165-182.
- [7] J. Heo, S. Kim, S. Ryu, D. Jang, Delocalized Plastic Flow in Proton-Irradiated Monolithic Metallic Glasses, Sci Rep. 6 (2016) 23244.
- [8] S. V Ketov, Y. H. Sun, S. Nachum, Z. Lu, A. Checchi, A. R. Beraldin, H. Y. Bai, W. H. Wang, D. V Louzguine-Luzgin, M. A. Carpenter, A. L. Greer, Rejuvenation of metallic glasses by non-affine thermal strain, Nature. 524 (2015) 200-203.
- [9] N. Miyazaki, M. Wakeda, Y. -J. Wang, S. Ogata, Prediction of pressure-promoted thermal rejuvenation in metallic glasses, Npj Comput. Mater. 2 (2016).
- [10] S. V Madge, D. V Louzguine-Luzgin, A. Kawashima, A. L. Greer, A. Inoue, Compressive plasticity of a La-based glass-crystal composite at cryogenic temperatures, Mater. Des. 101 (2016) 146-151.
- [11] D. Grell, F. Dabrock, E. Kerscher, Cyclic cryogenic pretreatments influencing the mechanical properties of a bulk glassy Zr-based alloy, Fatigue Fract. Eng. Mater. Struct.41 (2018) 1330-1343. [12] J. Ding, S. Patinet, M. L. Falk, Y. Q. Cheng and E. Ma, Soft spots and their structural signature in a metallic glass, Proc. Nat. Acad. Sci. 111 (2014) 14052-14056.

- [13] J. Zylberg, E. Lerner, Y. Bar-Sinai and E. Bouchbinder, Local thermal energy as a structural indicator in glasses, Proc. Nat. Acad. Sci. 114 (2017) 7289-7294.
- [14] A. S. Argon, Plastic deformation in metallic glasses, Acta Metall. 27 (1979) 47-58.
- [15] M. L. Falk, J. S. Langer, Dynamics of viscoplastic deformation in amorphous solids, Phys. Rev. E. 57 (1998) 7192-7205.
- [16] A. S. Argon, L. T. Shi, Development of visco-plastic deformation in metallic glasses, Acta Metall. 31 (1983) 499-507.
- [17] C. A. Schuh, A. C. Lund, T. G. Nieh, New regime of homogeneous flow in the deformation map of metallic glasses: elevated temperature nanoindentation experiments and mechanistic modeling, Acta Mater. 52 (2004) 5879-5891.
- [18] Y. Fan, T. Iwashita, T. Egami, How thermally activated deformation starts in metallic glass, Nat Commun. 5 (2014) 5083.
- [19] J. D. Ju, D. Jang, A. Nwankpa, M. Atzmon, An atomically quantized hierarchy of shear transformation zones in a metallic glass, J. Appl. Phys. 109 (2011) 53522.
- [20] X. D. Wang, B. Ruta, L. H. Xiong, D. W. Zhang, Y. Chushkin, H. W. Sheng, H. B. Lou, Q. P. Cao, J. Z. Jiang, Free-volume dependent atomic dynamics in beta relaxation pronounced Labased metallic glasses, Acta Mater. 99 (2015) 290-296.
- [21] S. W. Provencher, A constrained regularization method for inverting data represented by linear algebraic or integral equation, Comput. Phys. Commun. 27 (1982) 213-227.
- [22] S. W. Provencher, CONTIN: a general purpose constrained regularization program for inverting noisy linear algebraic and integral equations, Comput. Phys. Commun. 27 (1982) 229-242.
- [23] R. S. Lakes, Viscoelastic Materials, Cambridge: Cambridge University Press, 2009.

- [24] H. B. Yu, X. Shen, Z. Wang, L. Gu, W. H. Wang, H. Y. Bai, Tensile plasticity in metallic glasses with pronounced beta relaxations, Phys. Rev. Lett. 108 (2012) 15504.
- [25] T. Lei and M. Atzmon, Unpublished reuslts.
- [26] M. Atzmon, J. D. Ju, Microscopic description of flow defects and relaxation in metallic glasses, Phys. Rev. E. 90 (2014) 42313.
- [27] H. S. Chen, The influence of structural relaxation on the density and Young's modulus of metallic glasses, J. Appl. Phys. 49 (1978) 3289-3291.
- [28] W. H. Wang, The elastic properties, elastic models and elastic perspectives of metallic glasses, Prog. Mater. Sci. 57 (2012) 487-656.
- [29] A. L. Greer, J. A. Leake, Structural relaxation and crossover effect in a metallic glass, J. Non. Cryst. Solids. 33 (1979) 291-297.
- [30] P. Das, D. Parmar, S. Sastry, Annealing glasses by cyclic shear deformation, arXiv preprint arXiv:1805.12476, 2018.